JOURNAL OF MATERIALS SCIENCE 37 (2002) 789–794

A nano-indentation study on the mechanical behaviour of the matrix material in an AA6061 - Al_2O_3 MMC

K. M. MUSSERT
Department of Materials Science, Delft University of Technology, Rotterdamseweg 137, 2628 AL Delft, The Netherlands

W. P. VELLINGA
Department of Mechanical Engineering, Eindhoven University of Technology, P.O. Box 513, 5600 MB Eindhoven, The Netherlands

A. BAKKER, S. VAN DER ZWAAG
Department of Materials Science, Delft University of Technology, Rotterdamseweg 137, 2628 AL Delft, The Netherlands
E-mail: S.VanderZwaag@stm.tudelft.nl

The nano-indentation technique is a suitable technique to measure hardness and elastic moduli profiles of AA6061 reinforced with Al_2O_3 particles, since it allows measurements of mechanical properties on a micrometer range. To investigate possible local variations in mechanical behaviour of the matrix material due to precipitation reactions being affected by the presence of ceramic reinforcements, nano-indentation tests were done on both metal matrix composite (MMC) as well as unreinforced reference material, in three different heat treatment conditions. Matrix response depends on heat treatment condition, but is approximately equal for the MMC and the base reference alloy. Due to the various imposed heat treatments, magnesium enrichment around the ceramic particles was observed, but hardness and elastic modulus of this interfacial layer could not be measured. To confirm the preferential segregation of Mg near the particle/matrix interface, linescans were made with a Scanning Electron Microscope (SEM) equipped with EDS (Energy Dispersive Spectrum) facilities. The limited width of the Mg rich zone explains the absence of typical 'interphase' indentations in this investigation. Hardly any differences in calculated elastic moduli and hardness values were found for the three heat treatment conditions investigated, when comparing results of AA6061 reference material with results of an AA6061 matrix in an MMC. This result is of great importance when modelling the mechanical behaviour of MMCs using the finite element method, since it permits the assumption that the MMC matrix material behaves similar to the same aluminium alloy without ceramic reinforcements.

1. Introduction

Macroscopic mechanical properties of MMCs are not only determined by the mechanical properties of the various constituents, but a considerable contribution is due to the behaviour of the particle/matrix interface. Stiffening and strengthening rely on load transfer across this interface, toughness is influenced by crack deflection and ductility is affected by relaxation of peak stresses near the interface [1]. Some investigators have found that, as result of a heat treatment, the matrix regions adjacent to the reinforcement may exhibit a higher dislocation density when compared with matrix material further away from the interface due to mismatch of the coefficients of thermal expansion (CTE) between the matrix and the ceramic reinforcements [2]. These CTE-dislocation effects influence the kinetics of precipitation. Matrix dislocations may act as nucleation sites for precipitates and a higher density facilitates precipitation formation. Furthermore, the dislocations may act as preferential paths for solute diffusion which can accelerate the ageing process [2–4].

Since the width of particle/matrix interfaces and the interparticle distances are of the order of micrometers, it is practically not possible to determine gradients in mechanical properties around the particles using conventional techniques. However, nano-indentation which measures the resistance to plastic deformation in very small volumes, may offer some indication of gradients in mechanical behaviour on the micrometer range. Because of this capacity, nano-indentation is often used to

measure thin hard films [5]. However, Leggoe *et al*. [6] and Das *et al*. [7] used the method to study aluminium-based particle reinforced MMCs. In the latter investigation, a distinction was made between indentations in a particle, interface or matrix. Electron probe microanalysis (EPMA), indicated that magnesium enrichment occurred in the interfacial region between the particle and the matrix and the width of this phase increased with ageing time. This magnesium enrichment has been attributed to the presence of a $MgAl_2O_4$ spinel which formed during fabrication and which gave rise to a layer of matrix material around the particles with high hardness. It is of great importance to investigate the occurrence of such an interfacial layer and its influence on the mechanical behaviour of the matrix material in an MMC compared to the matrix response to heat treating in the base reference alloy.

In this investigation, nano-indentation testing is used to measure the hardness and elastic moduli profiles of AA6061 reinforced with Al_2O_3 in three different heat treatment conditions. Results are compared with nano-indentation measurements on unreinforced AA6061 in the same three heat treatment conditions, to investigate possible changes in the mechanical behaviour of the matrix material due to the presence of the ceramic reinforcement. When hardly any differences are to be found in the mechanical behaviour of the MMC matrix material in comparison with the AA6061 reference alloy, finite element calculations on MMCs are simplified since the matrix behaviour can then be assumed to behave the same as that of the aluminium alloy without ceramic reinforcements.

2. Materials used

The MMC used was produced via the stir casting process by Duralcan USA and consists of an AA6061-based alloy and 20 vol% Al_2O_3 particles. AA6061, a widely used typical extrusion alloy containing Mg and Si as the principal alloying elements, is a very suitable alloy as matrix for MMCs since its properties can be adjusted by a suitable heat treatment. An unreinforced AA6061 alloy of almost identical composition was used as the reference system. The compositions of both the MMC matrix alloy and the reference AA6061 are listed in Table I.

To produce known and reproducible precipitation structures in the AA6061 material as well as the MMC matrix material, all specimens were solutionized for 2 hours at 530°C followed by water quenching. In order to generate distinctly different precipitates in the matrix material, three different heat treatments were imposed making use of the results of a recent study on the precipitation kinetics in AA6061-based MMCs [8]. In that study, DSC curves were obtained for both homogenised AA6061 MMC and the reference alloy at a fixed heating rate of 5°C/min (see Fig. 1). In this figure, the peaks at around 60°C (labelled A) are related to Si clustering, those at around 230°C (labelled B) to β'' formation, those at around 280°C (labelled C) to β' formation and those at around 480°C (labelled D) to β-Mg_2Si formation.

TABLE I Chemical composition of the materials tested in weight percentage

Material	Mg	Si	Cu	Ni	Mn	Cr	Fe	Ti
AA6061	0.890	0.628	0.338	0.011	0.104	0.104	0.364	0.030
MMC	1.107	0.446	0.229	0.006	0.001	0.090	0.045	0.012

TABLE II Water quench temperatures for the AA6061 alloy and the MMC

Material	Temperature [°C]
AA6061-B	256
AA6061-C	309
MMC-B	254
MMC-C	300

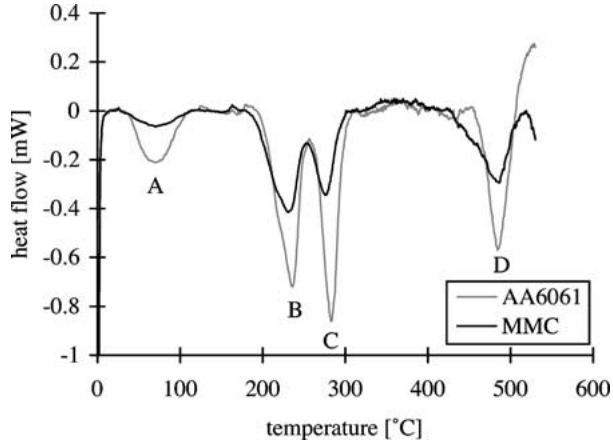

Figure 1 DSC traces of AA6061 and the Duralcan AA6061 with 20 vol% Al_2O_3 particles, heating rate 5°C/min [8].

In the present work, the condition of a matrix containing a maximum amount of β'' precipitates was created by linear heating the samples to a temperature of 255°C (condition B), using a heating rate of 5°C/min. A matrix containing a maximum amount of β' precipitates was created by linear heating the samples to a temperature of 305°C (condition C), using a heating rate of 5°C/min. To account for small differences in precipitation kinetics in the MMC and the reference alloy, the maximum annealing temperatures were adjusted according to Table II. The third heat treatment condition was an as-received T6-condition for the MMC, which consisted of solutionizing followed by 8 hours holding time at 175°C and an as-received T651-condition for the AA6061 alloy, which had additional stretching of ∼2% before artificially ageing.

3. Nano-indentation procedure

The mechanical properties of both matrix material and MMC were investigated with a nano-indenter developed at Eindhoven University of Technology which continuously measures force and displacement as an indentation is made. The indenter in this instrument is a Berkovich diamond three-sided pyramid with a nominal angle of 65.3° and an area-to-depth function which is the same as that of a Vickers indenter. For each sample at least ten indentations were made with a maximum load of 30 mN and the indentations

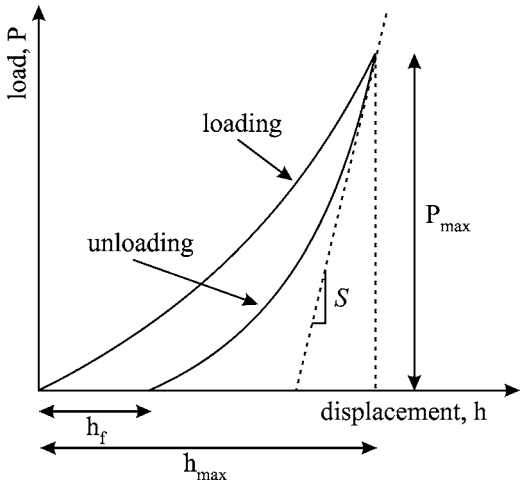

Figure 2 Schematic representation of a loading-unloading curve for a nano-indentation measurement; P_{max} is the load at maximum indentation, h_{max} is the indenter displacement at peak load, h_f is the final depth of the contact impression after unloading and S is the initial unloading stiffness.

were separated by 20 μm. On the MMC sample in T6-condition, the maximum applied load for the indentations was 100 mN. The samples had to be polished to 0.25 μm for the indenter to trace the surface, since any roughness affects the indentation curve. From the data obtained during unloading of the indentation, elastic displacements can be determined and from these measurements the elastic modulus, E, can be calculated. Furthermore, by removing the elastic contribution from the total displacement, the hardness, H, can be calculated. A schematic diagram of a typical loading-unloading curve is shown in Fig. 2.

The displacement plotted in this figure represents the total displacement of the indenter relative to the initial position. This value is composed of both elastic and plastic displacements. An important observation concerns the shape of the hardness impression after the indenter is unloaded and the material elastically recovers [9]. In metals it turned out, that the impression formed by a conical indenter is still conical, but with a larger included tip angle. Doerner and Nix [10] observed that during the initial stages of unloading, the area of contact remains constant as the indenter is unloaded. The unloading stiffness is then related to the elastic modulus and the projected area of the elastic contact, A, through the following relationship:

$$S = \left(\frac{\mathrm{d}P}{\mathrm{d}h}\right)^{\text{unloading}}_{P=P_{\max}} = \frac{2}{\sqrt{\pi}} E_{\mathrm{r}} \sqrt{A} \tag{1}$$

where E_r is the reduced elastic modulus as defined in the following equation:

$$\frac{1}{E_{\mathrm{r}}} = \frac{(1-\nu^2)}{E} + \frac{\left(1-\nu_i^2\right)}{E_i} \tag{2}$$

where E and ν are the Young's modulus and Poisson's ratio for the specimen and E_i and ν_i are the same parameters for the nano-indenter material. To determine the contact area at peak load, Oliver and Pharr [9] proposed a new method of analysis, since the behaviour of materials when indented by a Berkovich indenter can not be described using the flat punch approximation [10]. Sneddon [11] has derived analytical solutions for punches of several geometries, including conical indenters. Like for the Berkovich indenter, the cross-sectional area of a conical indenter varies as the square of the depth of contact and its geometry is singular at the tip. Therefore, Oliver *et al.* [9] assume that the behaviour of a conical indenter gives a better description of the elastic unloading of an indentation made with a Berkovich indenter. The area of contact at peak load is then determined by the geometry of the indenter and the depth of contact, h_c. The indenter geometry can be described by an area function $F(h)$ which relates the cross-sectional area of the indenter to the distance from its tip, h. Given that the indenter itself does not deform significantly, the projected contact area at peak load can then be calculated from the relation:

$$A = F(h_{\mathrm{c}}) \tag{3}$$

In addition to the elastic modulus, the hardness, H, defined as the applied load divided by the projected area of contact between the indenter and the sample can now be calculated:

$$H = \frac{P_{\max}}{A} \tag{4}$$

4. Results and discussion

Typical loading-unloading indentation curves acquired for the MMC in T6 condition are shown in Fig. 3.

In this figure, shallow penetration curves are attributed to indentations in particles and deep penetrations to those in the matrix. In contrast to Das *et al.* [7] this investigation did not reveal a third distinct group of indentations representing an existing 'interphase' between particle and matrix, for any of the heat treated MMCs. Little variation is observed for the particle indentations, more so for the matrix indentations. Indentation curves with deviant shapes were excluded from further interpretation. These curves were either a result of indentations in matrix material with underlying particles near the surface, indentations on particle-edges

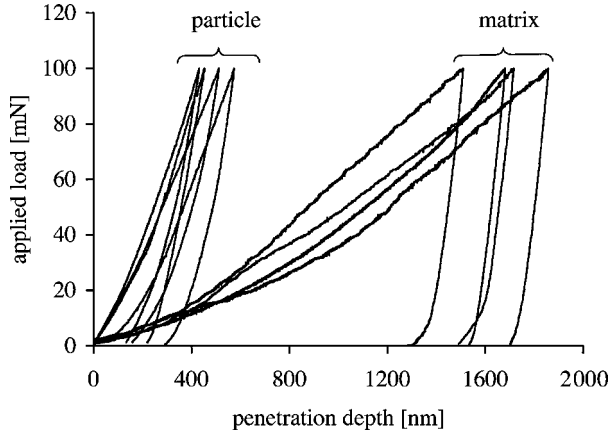

Figure 3 Indentation loading-unloading curves for an Al_2O_3 particle reinforced AA6061 MMC in T6 condition.

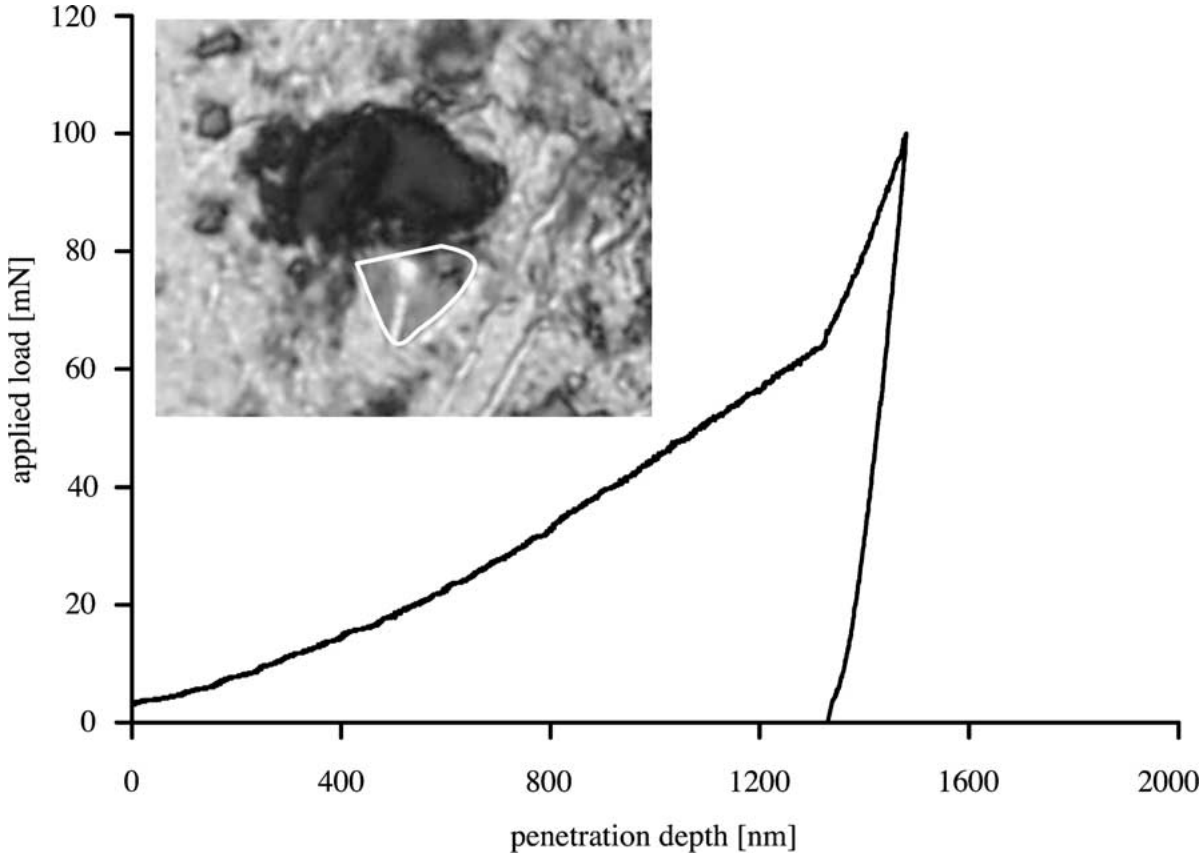

Figure 4 Indentation loading-unloading curve for an indent partially in the matrix and partially in a particle; the indentation is accentuated with a white line.

whereby the indenter slided off, or they were due to surface roughness of the sample. The latter is hard to overcome when investigating MMCs, since it turned out to be extremely difficult to level an MMC sample surface. A more detailed analysis of the shape of the indentation curves in relation to the position of neighbouring particles, showed a perfect example of a deviating curve which can be related to the indenter sliding off the ceramic particle, see Fig. 4.

Using dark field optical microscopy, most indentations in matrix material could be tracked down, whereas indentations in ceramic particles could not be found. After locating the position of the indentations in the matrix material with dark field, it was possible to switch to bright field and make photographs for further interpretation. Since the indentations in the MMC in T6 condition were made with a maximum load of 100 mN, the identification of the indentations was the easiest compared to the other MMCs and Fig. 5 shows such an indentation in the matrix.

Since Mg enrichment of an interfacial region would lead to magnesium depletion in the matrix further away from the particles and thus reduce the age hardening effects in these regions [7], this would lead to a correlation between the measured hardness in the matrix and the distance to the nearest reinforcing particle. For the successful matrix indentations, this distance was measured using the photographs made with bright field optical microscopy, but no correlation between hardness and distance to the nearest Al_2O_3 particle was found. From Fig. 5, it can be seen that an indentation with a maximum load of 100 mN takes up approximately 10 μm. Although measurements by Das *et al*. [7] were done with a maximum load of 30 mN, it is hard to understand that they were able to measure exactly in this interfacial layer without encountering problems similar to those found in this investigation as shown in Fig. 4.

To confirm the preferential segregation of Mg near the particle/matrix interface, linescans were made with a SEM equipped with EDS (Energy Dispersive Spectrum) facilities. Fig. 6 shows such a linescan for the MMC material in the T6 condition. The box diagram at the top of the figure shows the translation of the chemical composition into the spatial distribution of the constituent phases; for example, the particles can be recognised by the increase of oxygen and the decrease of aluminium. Clear indications of Mg enrichment near particles were obtained. The average thickness of this Mg rich zone could not be established exactly, but was estimated to be approximately 4 μm. Such a value is in good agreement with data by Das *et al*. [7], who reported values ranging from 2–5 μm depending on annealing time. The limited width of the Mg rich zone explains the absence of typical 'interphase' indentations in our work, but also raises serious questions about the correctness of the 'interphase' indentations as reported by Das *et al*. This thought is also supported by the fact that the Mg content in the MMC investigated here is even higher than that in both MMCs investigated by Das *et al*. They investigated two MMCs, one consisting of AA6061 reinforced with 15 vol% angular Al_2O_3 particles and the other was reinforced with 20 vol% spherical Al_2O_3 particles. The first MMC contained

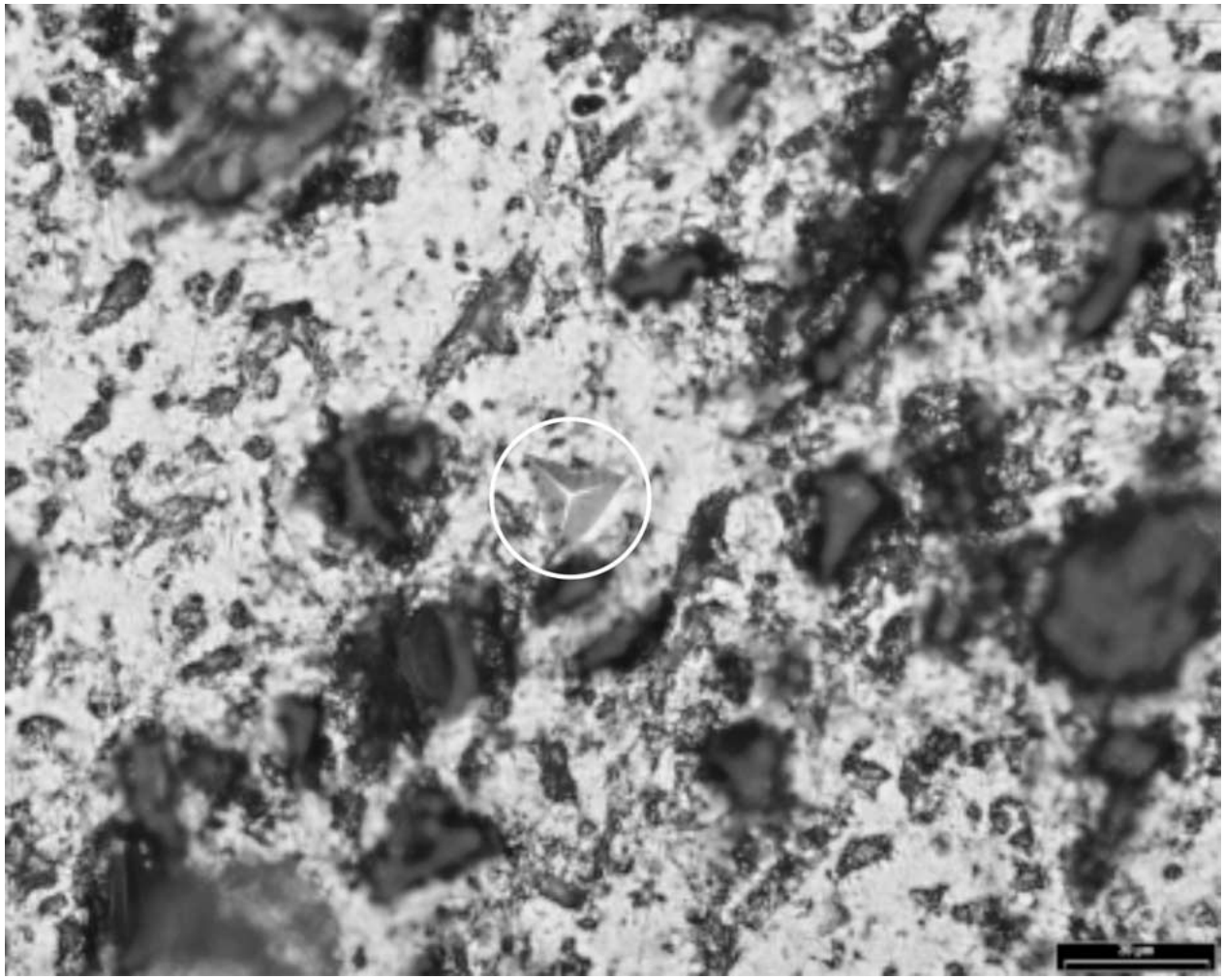

Figure 5 An example of an indentation in MMC matrix material in T6 condition.

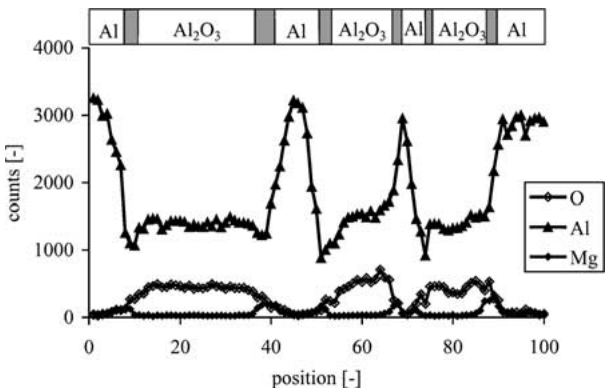

Figure 6 Linescan on AA6061-based MMC with 20 vol% Al_2O_3 particles in T6 condition; Mg enrichment is represented with the grey boxes in the upper bar.

0.752 wt% Mg and the latter 0.704 wt% Mg, whereas our MMC contained 1.107 wt% Mg.

Average elastic moduli and hardness values calculated for both the MMC and matrix material in all three heat treatment conditions are given in Table III. In the case of MMCs a distinction between matrix and particles could be made. The elastic moduli were determined from the linear fit to the initial points of the unloading part of the indentation curves and the hardness values were determined from the maximum force and plastic depth of the penetrations. In accordance with Das *et al*. [7], the calculated data in Table III exhibits a relatively small scatter for indentations in the matrix, but the data for the Al_2O_3 particles show a much wider scatter. This is thought to be due to the presence of cracks and pores in the particles and the high hardness of the material itself.

The elastic moduli of the particles were lower than those reported in the literature, i.e. approximately 380 GPa [12, 13]. Since the elastic modulus in the nanoindentation experiments is determined by a linear fit to the initial points of the unloading curve, an underestimation might be a result of a stronger curvature in the unloading curve for indentations in the particles. However, another plausible explanation may be the fact that the particles are embedded in a soft matrix. So, when an indentation in a particle is made, the soft material underneath the particle will reduce the apparent elastic modulus value.

When analysing the hardness data and indentation curves for the MMC matrix material and the unreinforced AA6061 alloy (taking into account the experimental error), practically the same trends in hardness as a function of heat treatment are observed. For the base AA6061 material Vickers microindentation measurements were performed too and Table III shows that the hardness values correspond well to those found using the nano-indentation technique. It can be seen that for the matrix and particles in the MMC and the reference

TABLE III Calculated elastic moduli and hardness values for matrix and particles in AA6061 with 20 vol% Al_2O_3 and in an AA6061 alloy as function of heat treatment

		Matrix			Particle	
Material	Condition	E [GPa]	H [GPa]	$H_{Vickers}$ [HV]	E [GPa]	H [GPa]
AA6061	T651	92 ± 4	1.14 ± 0.05	100 ± 2		
	B	89 ± 4	1.20 ± 0.04	112 ± 4		
	C	90 ± 3	0.99 ± 0.05	84 ± 2		
AA6061 +	T6	91 ± 6	0.97 ± 0.17		214 ± 44	14 ± 4.5
20 vol%	B	88 ± 2	1.17 ± 0.03		197 ± 53	15 ± 3.5
Al_2O_3	C	90 ± 10	1.03 ± 0.05		213 ± 38	11 ± 0.9

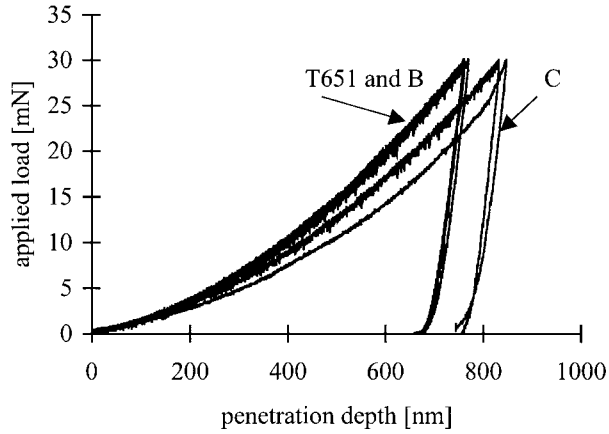

Figure 7 Comparison of the shapes of the indentation curves in the various heat treatment conditions; black lines represent the AA6061 alloy and grey lines the matrix of the MMC.

alloy the highest hardness values are obtained in condition B when compared with conditions C, T651 and T6.

Unlike the cited literature [5, 7, 14], no indication of significantly different mechanical behaviour of matrix material near a ceramic particle was found in this investigation. Hence, the shapes of the indentation curves for the MMC matrix and unreinforced AA6061 reference material for corresponding heat treatments can be compared in detail, see Fig. 7. Average curves for AA6061 in T651 and B condition show a perfect overlap with the MMC in B condition (the MMC in T6 condition was left out here since this was indented with a load of 100 mN). Taking into account the small differences in yield strength and hardening exponent determined for these two conditions from tensile testing experiments, this good overlap is not surprisingly, i.e. the yield strengths for T651 and B condition are 295 MPa and 328 MPa respectively and the hardening exponents are 15.8 and 15.6 respectively [15].

In the C condition the loading curves for both AA6061 and the MMC vary somewhat, but the unloading curves again show a good overlap. The fact that these curves differ from the T651 and B condition can also be related to the yield strength and the hardening exponent of this heat treatment condition which are much lower, i.e. 200 MPa and 7.9 respectively.

The fact that hardly any differences are found in the mechanical behaviour of the MMC matrix material in comparison with the AA6061 reference alloy, makes it permissible to perform finite element calculations in which the matrix behaviour is assumed to be the same as that of the aluminium alloy without ceramic reinforcements.

5. Conclusions

- Hardness and elastic moduli of matrix and particles in aluminium-based MMCs can be determined using the nano-indentation technique, but one should be cautious about the exact values found.
- Although Mg enrichment was observed in this investigation, it was not possible to measure the hardness and the elastic modulus of this interfacial layer as a function of the various heat treatment conditions.
- When comparing results of AA6061 reference material with the behaviour of an AA6061 matrix in an MMC in three different heat treatment conditions, it turned out that there are hardly any differences in calculated elastic moduli and hardness values. So, when modelling the mechanical behaviour of MMCs using the finite element method it is permissible to assume the MMC matrix behaving similar as the same aluminium alloy without ceramic reinforcements.

References

1. T. W. CLYNE and P. J. WITHERS, "An Introduction to Metal Matrix Composites" (Cambridge University Press, Cambridge, Great Britain, 1993).
2. R. J. ARSENAULT and N. SHI, *Materials Science and Engineering* **81** (1986) 175.
3. I. DUTTA, S. M. ALLEN and J. L. HAFLEY, *Metallurgical Transactions A* **22A** (1991) 2553.
4. T. DAS, P. R. MUNROE and S. BANDYOPADHYAY, *J. Mater. Sci.* **31** (1996) 5351.
5. E. SÖDERLUND, I. REINECK and D. J. ROWCLIFFE, *J. Mater. Research* **9** (1994) 1683.
6. J. W. LEGGOE, X. Z. HU, M. V. SWAIN and M. B. BUSH, *Scripta Metallurgica & Materialia* **31** (1994) 577.
7. T. DAS, P. MUNROE, S. BANDYOPADHYAY, T. BELL and M. V. SWAIN, *Materials Science and Technology* **13** (1997) 778.
8. S. P. CHEN, K. M. MUSSERT and S. VAN DER ZWAAG, *J. Mater. Sci.* **33** (1998) 4477.
9. W. C. OLIVER and G. M. PHARR, *J. Mater. Research* **7** (1992) 1564.
10. M. F. DOERNER and W. D. NIX, *ibid.* **1** (1986) 601.
11. I. N. SNEDDON, *International Journal of Engineering Science* **3** (1965) 47.
12. D. J. LLOYD, *International Materials Reviews* **39** (1994) 1.
13. I. A. IBRAHIM, F. A. MOHAMED and E. J. LAVERNIA, *J. Mater. Sci.* **26** (1991) 1137.
14. J. S. ZHANG, X. J. LIU, H. CUI, Z. Q. SUN and G. L. CHEN, *Scripta Materialia* **35** (1996) 1115.
15. K. M. MUSSERT, PhD Thesis, T. U. Delft, 2000.

Received 29 November 2000
and accepted 3 August 2001